7 History of passive remote sensing of aerosol from space

Omar Torres and Lorraine A. Remer

7.1 First observations from space

The earliest views of aerosol from space came from Russian cosmonauts who took handheld photographs of Earth and Earth's atmosphere through the windows of orbiting spacecraft in the early 1960s (Lazarev et al., 1987). From these photographs we could see for the first time the bluish haze that covered polluted regions and the dust emitted from deserts. The pictures showed that these hazes were inhomogeneous and temporally inconsistent, but quantitative information was missing until the first spectroscopic measurements of the atmosphere were obtained in 1970 by Soyuz-9 cosmonauts using handheld spectrometers. Thus, the era of space-based aerosol remote sensing had begun.

The first stratospheric aerosol measurement on record was obtained during the joint Soviet-American mission in 1976 using a handheld sunphotometer. On this mission the Stratospheric Aerosol Measurement (SAM) was carried out as a proof-of-concept by the Apollo-Soyuz Test project that made use of solar occultation observations to quantify stratospheric aerosols in terms of the vertical distribution of aerosol extinction coefficient (Pepin and McCormick, 1976; see Chapter 4).

Aerosol measurements from unmanned platforms in space were obtained for the first time by the Multi Spectral Scanner (MSS) sensor onboard the Earth Resources Technology (ERTS-1) satellite launched in 1972 (Griggs, 1975; Fraser, 1976; Mekler et al., 1977). Observations from the Advanced Very High Resolution Radiometer (AVHRR) on the TIROS-N satellite deployed in October 1978 were used to generate the first operational aerosol product. Since then, a long list of spaceborne sensors have been used to detect and characterize aerosols. For three decades (1970–2000) a majority of satellite-based aerosol observations were obtained by sensors designed and deployed for other purposes. The cre-

J. Lenoble et al. (eds.), *Aerosol Remote Sensing*, Springer Praxis Books,
DOI 10.1007/978-3-642-17725-5_7, © Springer-Verlag Berlin Heidelberg 2013

ative use of these measurements to infer aerosol properties paved the way for the eventual development and deployment of more accurate sensors specifically designed to measure aerosol properties.

This chapter describes the different methods to retrieve aerosol information applied to the "heritage sensors", those in flight before the onset of the Earth Observation System (EOS) era. The "modern sensors", aboard satellites that began collecting data in 2000 are described in Chapter 8. Many of the heritage sensors are still in operation, still extending time series of aerosol measurements, as of 2012.

7.2 Measuring stratospheric aerosols using solar occultation measurements

The solar occultation technique is a simple method of measuring vertical profiles of atmospheric extinction from Earth orbit using the sun as a light source. This is analogous to ground-based sunphotometry. See Chapter 4 and Figure 4.4 for a description of how the instrument observes the attenuated sunlight through the upper atmosphere for every sunset and sunrise observed. Typically the spacecraft orbits the Earth approximately once every 90 minutes or 16 times per day, depending on orbital parameters. Since each orbit provides two measurement opportunities, the sensor can acquire 32 separate measurements during each 24-hour period at different geographical locations over the Earth depending on the spacecraft orbit. The number of measurement opportunities and the geographical coverage can be increased if measurements are made during both lunar and solar occultation events.

Following the successful SAM test (Pepin and McCormick, 1976), the first satellite-based long-term monitoring program of the atmospheric aerosol load started with the deployment in 1978 of the SAM II sensor aboard the Nimbus 7 spacecraft. SAM II provided vertical profiles within the stratosphere of aerosol extinction at 1.064 μm in both the Arctic and Antarctic polar regions. The SAM II data coverage began on 29 October 1978 and extended through 18 December 1993, at which time SAM II was no longer able to track the sun. The discovery of Polar Stratospheric Clouds (PSCs) (McCormick et al., 1982), and the observation of the formation and evolution of the stratospheric aerosol layer in the aftermath of the El Chichon eruption are among the main scientific contributions of the SAM II program. The first multiyear climatology of PSCs was developed based on SAM II observations (Poole and Pitts, 1994). Nitric acid trihydrate PSCs were later found to play a critical role in the heterogeneous chemistry process leading to the formation of the stratospheric ozone hole (Molina, 1991 and references therein).

The Stratospheric Aerosol and Gas Experiment (SAGE I) on the Applications Explore Mission-2 (AEM-2) satellite was designed to monitor the evolution of the stratospheric ozone layer using solar occultation. To account for aerosol effects on the ozone inversion process, the vertical distribution of the stratospheric aerosol load was also measured in terms of particle extinction coefficient at 0.450 and 1.00 μm. SAGE I operated between 1979 and 1981 and provided a description of the global background stratospheric aerosol

load (Kent and McCormick, 1984) that complemented the SAM II measurements polar coverage. SAGE I provided the reference state of the stratospheric aerosol load prior to the series of volcanic eruptions that started in 1982 with the eruption of El Chichon in April 1982.

The short-lived but successful SAGE I stratospheric monitoring program was followed by the launch of the SAGE II sensor on the Earth Radiation Budget Satellite (ERBS) in March 1984. SAGE II provided the scientific community with a global depiction of the distribution of stratospheric aerosol, ozone, water vapor and nitrogen dioxide over a period of 21 years. The SAGE II record of aerosol extinction at four wavelengths from the UV to the near IR is the longest continuous aerosol record from the same sensor. During this lengthy time series the sensor observed the decay of the El Chichon aerosol layer as well as the formation and dissipation of the Pinatubo aerosol layer following the 1991 eruption. The SAGE III/Meteor-3M satellite mission operated as a joint partnership between NASA and the Russian Aviation and Space Agency (RASA). SAGE III was launched onboard a Meteor-3M spacecraft in December 2001. It measured aerosol extinction coefficients at nine wavelengths between 0.384 and 1.545 μm (Thomason et al., 2010 and references therein). The Meteor-3M mission, along with the SAGE III mission, was terminated in March 2006.

7.3 El Chichon and Pinatubo volcanic eruptions

The combined set of solar occultation observations by SAGE (1979–1981), SAM II (1978–1993) and SAGE II (1984–2005) were used to continuously characterize the evolution of the stratospheric aerosol load during a 27-year period during which the two largest volcanic eruptions of the last century took place. SAGE and SAM II measurements characterized the conditions of minimum stratospheric aerosol load prior to the April 1982 eruption of El Chichon. SAM II and SAGE II monitored the decay of the El Chichon stratospheric sulphuric acid aerosol layer. SAGE II mapped the entire lifetime of the stratospheric aerosol layer resulting from the Pinatubo eruption in June 1991, the largest volcanic eruption of the last 30 years, that greatly perturbed the stratospheric aerosol layer (Lambert et al., 1997).

Other instruments with aerosol sensing capability onboard the Upper Atmospheric Research Satellite (UARS) launched in September 1991 about three months after the massive Pinatubo volcanic eruption (Reber et al., 1993) contributed to the characterization of the Pinatubo aerosol layer. UARS, a stratospheric chemistry mission included the Cryogenic Limb Array Etalon Spectrometer (CLAES), the Halogen Occultation Experiment (HALOE), and the Improved Stratospheric and Mesospheric Sounder (ISAMS) sensors equipped to measure vertical distribution of aerosols in the stratosphere to account for aerosol scattering effects in the retrieval of concentrations of chemical species in the upper atmosphere. CLAES measured aerosol extinction profiles at 8 IR channels and operated between 1991 and 1993 (Roche et al., 1993). HALOE operated from 1991 to 1997 and was one of the most successful UARS instruments. Making use of the solar occultation approach to sound the stratosphere, mesosphere, and lower thermosphere, HALOE measured vertical profiles

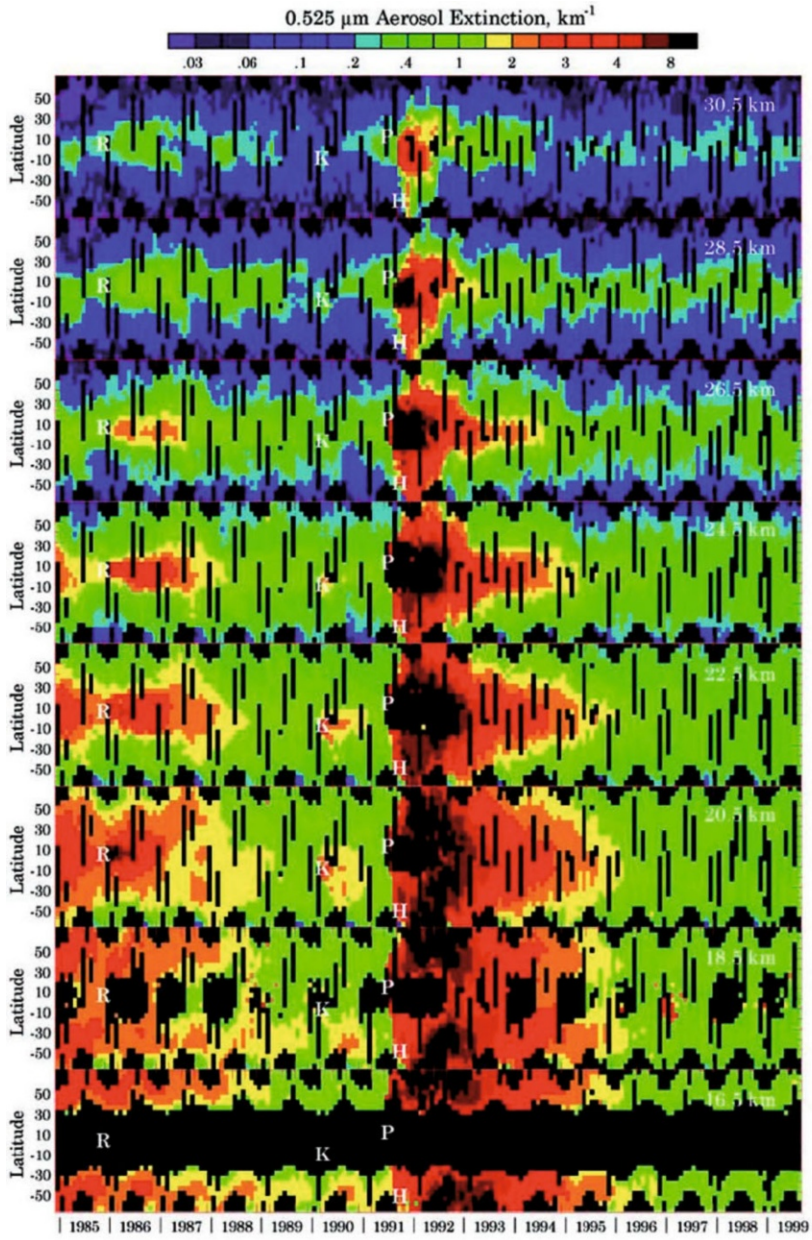

Figure 7.1 Zonally averaged 0.525 μm aerosol extinction at 30.5, 28.5, 26.5, 24.5, 22.5, 20.5, 18.5 and 16.5 km. The letters repeated in each frame mark the latitude and time of the Ruiz (R), Kelut (K), Pinatubo (P) and the Hudson (H) eruptions. From Bauman et al. (2003b), reprinted with permission from the American Geophysical Union.

of atmospheric ozone (O_3), hydrogen chloride (HCl), hydrogen fluoride (HF), methane (CH_4), water vapor (H_2O), nitric oxide (NO), nitrogen dioxide (NO_2), temperature, and IR aerosol extinction profiles (Russell et al., 1993). The ISAMS (Taylor et al., 1993) instrument measured aerosol extinction at 6.21 and 12.1 μm from September 1991 to July 1992.

The 15-year [1985–1999] record of the global stratospheric aerosol load as seen by the SAGE II and CLAES sensors (Bauman et al., 2003) is shown in Figure 7.1. The record starts with the remaining effects of the 1982 El Chichon eruption, enhanced in 1986 by the El Ruiz eruption, a much less significant but still important source of statospheric aerosol. The effect of the massive 1991 Pinatubo eruption is readily apparent at all levels between 16.5 and 30 km. The return to background levels takes place by early 1997 at the lowest altitude shown.

Attempts were also made to monitor the evolution of the Pinatubo aerosol layer using nadir observations by the AVHRR and TOMS sensors (algorithms described below). Stowe et al. (1992) and Long and Stowe (1994), studied the progression of the global Pinatubo aerosol layer using NOAA-11 AVHRR observation at 0.63 μm. The Pinatubo aerosol layer also had a significant effect on the remote sensing of atmospheric parameters such as the total column ozone amount derived by the Total Ozone Mapping Spectrometer (TOMS) on the Nimbus-7 satellite. The large signal of the aerosol effect on the retrieved ozone amounts (Bhartia et al., 1993) was used to indirectly estimate the magnitude of the tropical stratospheric aerosol load in the UV as a function of time (Torres et al., 1995).

7.4 Total column aerosol retrieval from reflected visible and near IR observations

As described in the previous section, aerosol characterization using solar occultation measurements have provided descriptions of the temporal and spatial variability of stratospheric aerosols, most of which are of natural origin. To properly account for the total atmospheric aerosol, however, it is necessary to include the troposphere where most anthropogenic aerosols reside. Thus, downward-viewing satellite measurements are required for total column aerosol retrieval.

Downward-viewing satellite retrievals are fundamentally different from solar occultation measurements in that they measure reflected solar radiation, not the direct beam attenuated through the upper atmosphere. This is represented by the radiance, rewritten here from Eq. (3.33a),

$$L(0,\mu,\varphi) = L_0(0,\mu,\varphi) + \frac{RF_0(\tau^*)T_t(\tau^*,\mu)}{(1-RS)}, \tag{7.1}$$

where $L(0,\mu,\varphi)$ is the measured upwelling radiance at the top of the atmosphere, composed of two parts. $L_0(0,\mu,\varphi)$ is called the path radiance and it represents radiance scattered into the satellite sensor's field of view from atmospheric constituents (aerosols or gases). The path radiance has had no interaction with the surface beneath and would be the upwelling

radiance of the atmosphere for a black surface. The second term on the right expresses the interaction of the radiance between the atmosphere and the surface (see Figure 3.4) that is later scattered into the sensor's field of view. Here $F_0(\tau^*)$ is the downward flux reaching a black surface, and T_t the total transmission function representing the total amount of direct plus diffuse radiation transmitted. R is the Lambertian surface reflectance and S the reflected flux at the bottom of the atmosphere called the spherical albedo of the atmosphere for illumination from below (Tanré et al., 1979).

The measured reflected radiance at the top of the atmosphere includes the combined effect of gaseous absorption and molecular scattering, aerosol scattering and absorption, cloud scattering and surface reflection. From this intertwined mixture of information the aerosol signal must be isolated and the competing effects must be accurately accounted for or altogether avoided in order to achieve accurate measurements of total column aerosol load.

The spectral choice and width of each spectral band to be used in the retrieval and the spatial resolution of the measurement are of great importance for aerosol retrieval. By choosing wavelengths in narrow spectral bands that correspond to the window regions of the solar spectrum, gas absorption can be avoided. Furthermore, avoiding other spectral bands that introduce uncertainty from surface features (i.e. ocean color) helps in the isolation of the aerosol signal. Since cloud interference with the observation must also be avoided, the spatial resolution must be sufficiently fine so that aerosols can be observed through clear holes in otherwise cloudy skies. As the technology of spaceborne sensors becomes more sophisticated, expanding to a broader spectral range, multiple angles and polarization, different strategies to avoid misinterpreting reflectance from clouds as reflectance from aerosol can be used instead of simply trying to avoid clouds. However, historically, cloud masking has been a critical component of all downward-viewing retrievals.

A major hurdle in aerosol retrieval is the treatment of bright surfaces whose contribution to the satellite-measured signal is significantly larger than the aerosol contribution. The separation of the small aerosol component from a significantly larger surface term is a large source of error if the surface reflective properties are not accurately characterized. For that reason the most accurate retrievals have been done over water surfaces at visible and near IR wavelengths, taking advantage of the very low reflectance of water in this spectral range. Retrieval algorithms that use low-reflecting backgrounds to infer aerosol properties from space observations are generically referred to as "dark-target" approaches and are physically based on interpreting *path radiance* in terms of aerosol optical depth (Kaufman and Sendra,1988). As $R \rightarrow 0$ in Eq. (7.1), $L(0,\mu,\varphi) \rightarrow L_0(0,\mu,\varphi)$. A parallel method developed to retrieve aerosol over bright land surfaces is based on adjacency effect or contrast reduction and is physically based on using *transmission* to infer aerosol properties (Tanré et al.,1988), described below in Section 7.4.3.

Aerosol retrieval algorithms that use observations of reflected radiance have been based on pre-calculated top-of-atmosphere reflectances assuming aerosol models characterized in terms of aerosol particle size distribution and composition (i.e. refractive index). A set of forward radiative transfer calculations is made for a variety of pre-defined aerosol models for the range of solar and sensor view angles expected to be encountered by the satellite observations. These calculations are made for a range of aerosol loadings. The result of the calculations is a set of reflected radiances at top-of-atmosphere, indexed by wavelength,

aerosol loading, solar and view geometry and by aerosol model, $L^{LUT}(\lambda,\tau,\mu_o,\varphi_o,\mu,\varphi,\text{model})$. The results of the forward calculations are generically referred to as look-up tables (LUT) and are permanently stored. During a retrieval, after a series of checks and modifications of the measured reflected radiance to obtain the aerosol reflectance clear of influence of clouds and gases, the procedure is to match the modified measured radiance, $L(0,\mu,\varphi)$ at wavelength, λ, to the output of the stored LUT for the solar and view angles of that particular measurement. When a match is found, the retrieval identifies the aerosol loading and, in some cases, certain parameters of the aerosol model that are not prescribed *a priori*. The main retrieved parameter is aerosol optical depth, which is the same as the vertically integrated extinction coefficient. Depending on how many wavelengths, angles and polarization states are used in the retrieval, the aerosol optical depth may be a function of wavelength. Aerosol retrievals using these LUTs are very sensitive to the choice of aerosol microphysical properties (i.e. particle size distribution and complex refractive index) as they ultimately determine the amount of scattered radiance reaching the satellite-borne sensor. The future of aerosol remote sensing will include more sophisticated sensors returning much more information of the viewed scene. There should be sufficient information in these multiwavelength, multiangle polarimeters to mathematically invert the aerosol characteristics without the burden of *a priori* assumptions about aerosol particle size distribution and complex refractive index. Historically, simply returning an accurate measure of aerosol loading, the aerosol optical depth, even in one wavelength, was a major step forward.

7.4.1 Retrieval of aerosols over the oceans using the dark target approach

The astronaut photographs of the Earth clearly demonstrated the severe impacts that the atmosphere would have on interpreting images of the Earth's surface from space and retrieving quantitative information on surface reflectance. Important satellite-based measures of Normalized Difference Vegetation Index (NDVI) and ocean color that had significant important applications for estimating terrestrial and marine bio-productivity, crop yields and early famine warnings, would be confused by changing aerosol in the atmosphere above the scene. These scenes would require atmospheric correction to obtain the surface reflectance, and fundamental to atmospheric correction would be the quantification of the aerosol loading. As atmospheric correction improved, so would remote sensing of aerosol. Aerosol remote sensing over ocean thus began with the need for atmospheric correction to retrieve true water-leaving radiances from the apparent reflectance. The basic work here was pioneered by Gordon and Wang (1994), and Fraser et al. (1997), and made use of earlier work by Griggs (1975). The by-product of oceanic atmospheric correction produced an aerosol product. Atmospheric corrections were applied to the Coastal Zone Color Sensor (CZCS) initially and then to the Sea-viewing Wide field of view Sensor (SeaWiFS). The same methods were adapted to specifically focus on aerosol retrieval and applied retroactively over the global oceans using satellite sensors never intended for aerosol retrievals.

The Earth Resources Technology Satellite – 1 (ERTS-1) and later Landsat-2 carrying the multispectral scanner (MSS) provided the first opportunity to derive aerosol optical depth over ocean from space (Griggs, 1975). ERTS-1 was launched in 1972 and the Landsat series continued the tradition with the last Landsat-7 launched in 1999 and the Landsat

continuation mission scheduled for launch in late 2012. Griggs (1975) was able to retrieve aerosol in three wavelengths: 0.55 μm, 0.65 μm and 0.75 μm, each matched independently to pre-calculated radiances in a LUT with *a priori* assumptions of aerosol size distribution, complex refractive indices and rough ocean surfaces. Other techniques were explored with MSS data including contrast methods that will be described in Section 7.4.3. Continuing efforts were made to derive aerosol from MSS and subsequent Landsat-borne instruments based on the Griggs (1975) dark target approach. None of these efforts ever produced an operational product. ERTS-1 and the later Landsat satellites were designed to observe vegetation and geological targets. Spatial resolution of the MSS sensor was 80 m, with later sensors such as the Thematic Mapper (TM) having a broader spectral range and even finer resolution. The result of this fine resolution imagery was a narrow swath of less than 200 km, insufficient to deliver a daily picture of the global aerosol system. Yet the fine resolution and multiple channels overwhelmed the electronic archiving capabilities of the time. Images were collected, but not stored unless a paying customer was identified. Almost all customers had land-based applications in mind for the imagery. Most views of the rela-

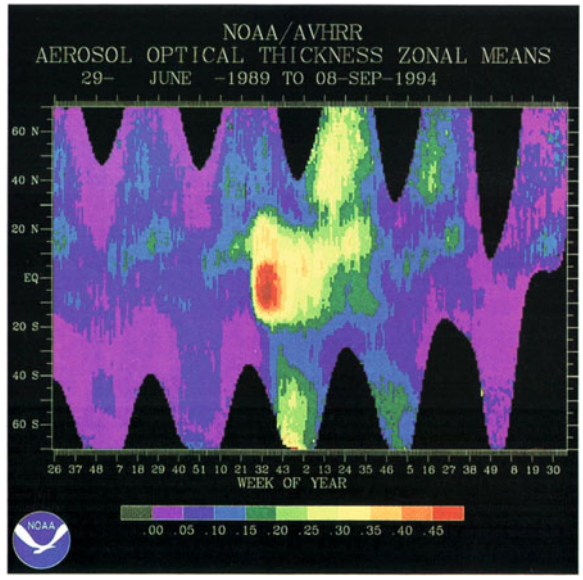

Figure 7.2 Latitudinally resolved time series of total aerosol optical depth at 0.50 μm retrieved from the AVHRR satellite using the first generation single channel retrieval. From Stowe et al. (1997). Reprinted with permission from the American Geophysical Society.

tively boring ocean were never saved, making a retroactive processing of Landsat data for ocean aerosol retrievals impossible. In the later years of the Landsat program, images were saved on a routine basis, but the motivation to retrieve aerosol information from these data on a routine basis never gained momentum, being replaced by the success of retrievals of sensors that could provide wide swath data and nearly global views of the aerosol system on a daily basis.

The Advanced Very High Resolution Radiometer (AVHRR) was the first sensor to support operational aerosol retrievals over oceans and provide daily views of the global aerosol system. AVHRR is a five-channel sensor (nominally 0.63 μm, 0.83 μm, either 1.6 μm or 3.7 μm, 11 μm and 12 μm) designed as a surface and cloud imager by NOAA/NESDIS for weather applications. Since its inception in 1978, three generations of AVHRR sensors have been flown onboard TIROS-N and the NOAA polar operational environmental satellites (POES). The solar reflectance bands centered at 0.63 and 0.83 μm have remained unchanged, providing the desirable temporal continuity for long-term environmental monitoring. AVHRR sensors have flown onboard TIROS-N, NOAA-6, through NOAA-12 and NOAA-14 to 17 satellites. The global coverage and moderate spatial resolution (1 km) made AVHRR an attractive instrument for operational aerosol retrievals. Even so, the instrument was not designed for aerosol retrievals and hurdles had to be overcome. The most significant challenge for AVHRR aerosol retrievals was to account for drift in the instruments' radiometric calibration. Various vicarious calibration methods were used to standardize instrument calibration (Holben et al., 1990; Vermote and Kaufman, 1995; Rao and Chen, 1996). The incentive to derive quantitative aerosol information from AVHRR increased once a reliable calibration was available.

Almost all of the aerosol information available from AVHRR is contained in the first two channels: 0.63 μm and 0.83 μm. There have been several strategies to make use of this aerosol information that we categorize as either single channel or two channel retrievals.

Single channel AVHRR retrieval approach

The single channel retrieval makes use of AVHRR Channel 1 (0.63 μm). The original algorithm assumes a Lambertian ocean surface with surface albedo of 0.015, and one aerosol model represented by a modified Junge particle size distribution equivalent to an Ångström exponent of 1.5 and complex refractive index of 1.5–0.0i (Rao et al., 1989; Stowe et al., 1990; Stowe et al., 1997). Note that the aerosol is assumed to be completely non-aborbing with ϖ_o=1 because the imaginary part of the refractive index is 0.0. The Ångström exponent of 1.5 is higher than the values of pure maritime aerosol reported by Smirnov et al. (2002). The retrieval procedure followed the typical dark target oceanic methods: masking clouds and sun glint, matching measured radiances in the 0.63 μm channel to pre-calculated values in the LUT for the particular solar and view angles of the scene in question, and retrieving the aerosol optical depth that was used to calculate the LUT top-of-atmosphere radiance. This algorithm was used to characterize the aerosol optical depth over the global oceans, identifying regions of heavy aerosol loading. An example of this product for the monthly mean aerosol optical depth in 1995 is shown in Figure 7.2. The algorithm applied to the long AVHRR time series that began in 1978 produced a data set that fully characterized the total aerosol optical depth of the Pinatubo eruption, similarly as to how the solar

occultation instruments had characterized the Pinatubo aerosol in the stratosphere (Figure 7.1).

The next generation single channel AVHRR retrieval kept the same basic procedure as at the beginning, but made several adjustments to the *a priori* assumptions used by the retrieval. First the Lambertian surface albedo was decreased considerably to 0.002, and a diffuse glint correction (Viollier et al.,1980; Gordon and Morel, 1983) was applied in lieu of the more modern usage of a non-Lambertian rough ocean surface model. Second, the Junge size distribution was replaced by a single mode lognormal size distribution that with a slightly modified complex refractive index produced an Ångström exponent of 0.6, more in line with measurements of maritime aerosol (Smirnov et al., 2002). The aerosol model remained entirely non-absorbing (Stowe et al., 1997; Ignatov et al.,1995b). This algorithm is used for generating the operational AVHRR aerosol products on a 1-degree global grid, known as AVHRR Pathfinder-Atmosphere (PATMOS) (Stowe et al., 2002; Jacobowitz et al., 2003) and is publicly available.

A continuing concern for all aerosol retrievals is the prospect of systematic cloud contamination in the retrieval product. The single channel algorithms use a cloud-clearing scheme that includes a series of radiance thresholds and a spatial variability test that examines the range of radiances in each 2 by 2 set of pixels. If the spread of radiances is two high in this set of 4 pixels, the 4 pixels are not used in the aerosol retrieval.

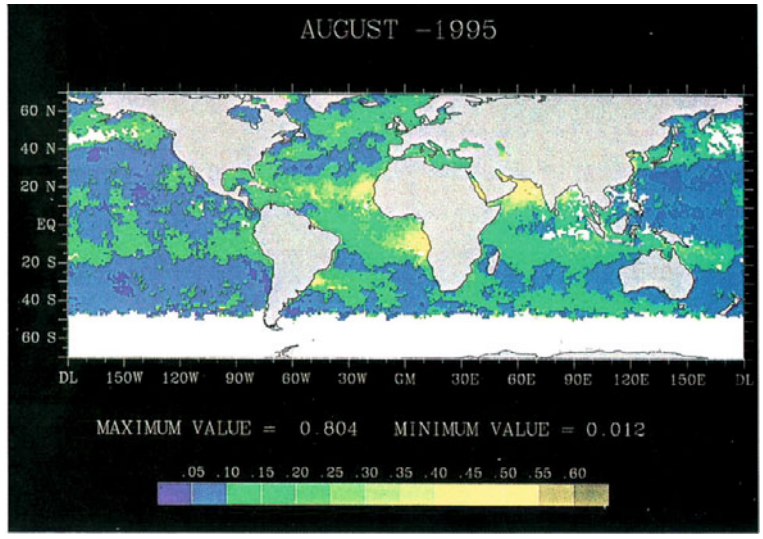

Figure 7.3 Total aerosol optical depth at 0.50 μm retrieved from the AVHRR satellite using the first generation single channel retrieval. From Stowe et al. (1997). Reprinted with permission from the American Geophysical Union.

Two channel AVHRR retrieval approach

A different approach for retrieving aerosol characteristics from AVHRR makes use of both solar channels on the AVHRR sensor (0.63 and 0.83 μm). Theoretically, the use of two channels allows for the calculation of the Ångström exponent or other parameter, which gives a qualitative measure of particle size. Dual-channel AVHRR algorithms have been developed by several groups (i.e. Higurashi and Nakajima, 1999; Mishchenko et al., 1999a). The methods include a LUT indexed by solar and view angles, aerosol optical depth and either Ångström exponent or a ratio between two particle modes that is directly proportional to Ångström exponent. These methods employ a rough ocean surface model with a globally fixed wind speed and a fixed complex refractive index (1.50 + 0.005i). Note the assumption here are that the particles are slightly absorbing with a nonzero imaginary part of the refractive index. All particles are assumed spherical in all cases. In one method the size distribution is composed of two lognormals, each fixed in mode radius and width, but allowed to increase or decrease in volume. The ratio between the two mode volumes is a free parameter in the retrieval (Higurashi and Nakajima, 1999). In another method the size distribution is a single mode modified power law with the exponent of the power law the free parameter (Mishchenko et al., 1999a). Sensitivity studies show little difference between the single mode and two-mode assumptions for particle size distributions (Mishchenko et al., 1999a). The Mishchenko et al. (1999a) algorithm was applied to the AVHRR record beginning in 1983 to produce the Global Aerosol Climatology Product (GACP) (Geogdzhayev et al., 2002), a publicly available time series of monthly mean aerosol optical depth and Ångström exponent on a 1 degree grid over the global oceans. Figure 7.4 shows the time-series of global mean aerosol optical depth derived by application of the dual-wavelength algorithm to AVHRR observations for the 1983-2001 period (Geogdzhayev et al., 2004).

The GACP product makes use of a modified ISCCP cloud detection in which the infrared tests are made more conservative (more likely to categorize the pixels as “cloudy”) and a test is added based on the ratio of the 0.63 μm and 0.83 μm radiances. The ratio test is based in the physics that clouds with their larger hydrometeors should be more spectrally neutral than the finer particle aerosols. In addition to the continuing concern about cloud contamination in the aerosol product, an important source of uncertainty in the two-wavelength AVHRR algorithm is the relative calibration error since there is no onboard calibration of the instrument.

7.4.2 Retrieval of aerosols over land using the dark target approach

The retrieval of aerosols over land is a much more difficult problem than its counterpart over ocean. The land surface tends to be both brighter and more variable than the ocean surface. Thus, while aerosol retrievals over oceans can model the radiance contribution from the surface with a high degree of certainty, the same is not true over land. One method used to derive aerosol over land is to find land surfaces that mimic the advantages of the ocean: relatively dark and homogeneous. Dark dense vegetation provides such an opportunity.

Kaufman and Sendra (1988) demonstrated an atmospheric correction technique for Landsat MSS images over land that would retrieve aerosol amounts using a dark target

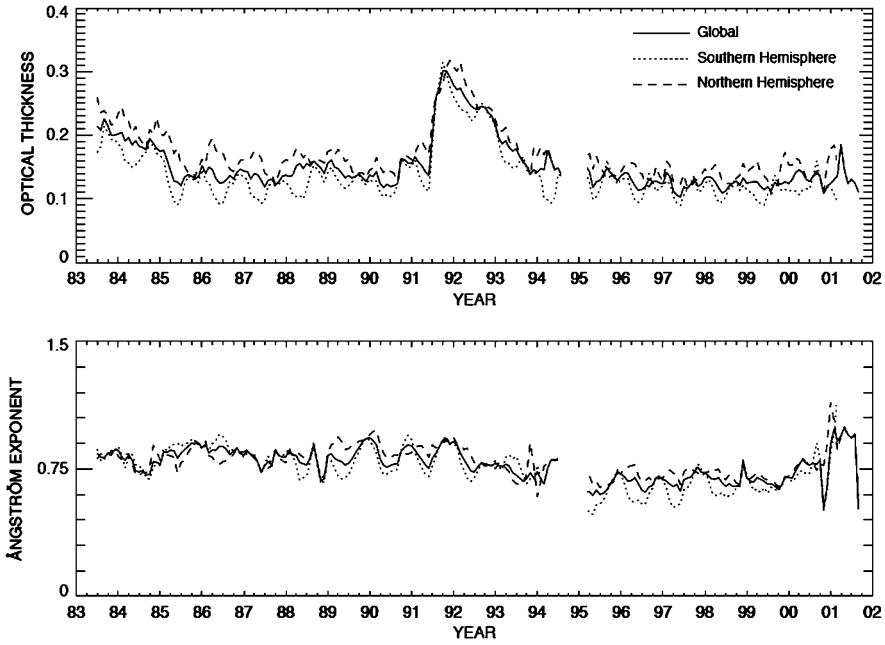

Figure 7.4 Multi-year AOD climatology over the global oceans derived by the two-channel AVHRR algorithm (top), and resulting Ångström exponent (bottom). From Geogdzhayev et al., 2004. Reprinted with permission from the Journal of Quantitative Spectroscopy and Radiative Transfer.

approach. The basis of a dark target approach is that aerosol will normally brighten a dark scene, causing the satellite-measured reflectance, $L(0,\mu,\varphi)$, to be larger than the surface reflected radiance (with reflectance R), mostly because of the large path radiance, $L_o(0,\mu,\varphi)$. This dark target approach identified the darkest pixels in the image, assumed the surface reflectance of these pixels (R), and then derived the aerosol amount based on that assumption. The approach then assumed that aerosol varied less over the image than the surface reflectance so that the aerosol amount determined from the darkest pixels could be applied to the whole image. The dark target approach worked because the error introduced by the surface reflectance assumption might be *relatively large*, but because of the small reflectances would be small in an absolute sense. There were two tricks to employing this method: finding the dark dense vegetation in the image and assuming the surface reflectance at the wavelengths of the retrieval.

The Normalized Difference Vegetation Index (NDVI) (Jordan, 1969; Tucker, 1979) uses the simple combination of the two reflective AVHRR channels to identify vegetation in the AVHRR image.

$$\text{NDVI} = \frac{\rho_{0.83} - \rho_{0.63}}{\rho_{0.83} + \rho_{0.63}}, \tag{7.2}$$

where ρ_λ is the reflectance given for a specific geometry as

$$\rho_\lambda = \frac{\pi L(\lambda)}{\mu_o E_o}, \tag{7.3}$$

for wavelength, λ, and where μ_o is $\cos(\theta_o)$ and E_o is the irradiance at top of the atmosphere. This is the reflectance defined in Eq.(3.62), denoted by S in Chapter 3. NDVI can be used to identify the dark vegetated pixels from which to derive the aerosol. The problem with NDVI is that as aerosol loading increases the measured reflectances increase. Because aerosol creates a spectrally dependent signature in the measured reflectances the value of $\rho_{0.83}$ increases more slowly than $\rho_{0.63}$ as aerosol loading increases. The result is that NDVI decreases as loading increases and it becomes difficult to identify the dark targets through the haze. To overcome this problem, techniques made use of the 3.7 μm band on AVHRR. The measured 3.7 μm reflectance includes components from thermal emission and from solar reflectance. The emissive part has to be removed from the measured signal in order to make use of the channel to find the dark targets. This is done using information from the AVHRR thermal band at 11 μm (Roger and Vermote, 1998). The advantage of using $\rho_{3.7}$ is that this relatively long wavelength is insensitive to fine aerosol types and can penetrate through the haze and 'see' the surface (Kaufman and Remer, 1994). Figure 7.5 shows insensitivity to aerosol by longer wavelength channels. For Landsat-4 Thematic Mapper (TM) and subsequent imagers such as MODIS, the 2.1 μm channel was used instead of the 3.7 μm channel because it had all the advantages of being insensitive to fine particles and yet did not require correction for thermal emission (Kaufman et al., 1997a).

The dark target approach was used with AVHRR radiances for specific studies (Kaufman and Nakajima., 1993; Vermote et al., 1996), but never adapted to produce an operational over land product. However, later it became the basis for one of the MODIS aerosol over land products (Kaufman et al., 1997b).

7.4.3 Retrieval of aerosols over land using the adjacency effect

The dark target approach will not work over scenes with bright surfaces, such as deserts. An alternative idea that was applied to deserts is based on how aerosol scatters light into the field of view from adjacent targets, this process is called the adjacency effect. The initial interest in the adjacency effect grew from the need to account for it as part of atmospheric correction. To obtain the true reflectance of a specific surface target, the light scattered into the scene from surrounding scenes would have to be removed. The amount of light scattered in the scene is dependent on the contrast between the target and surrounding targets, and also the aerosol loading and particle properties (Mekler and Kaufman, 1980; Kaufman and Fraser, 1983a and 1983b).

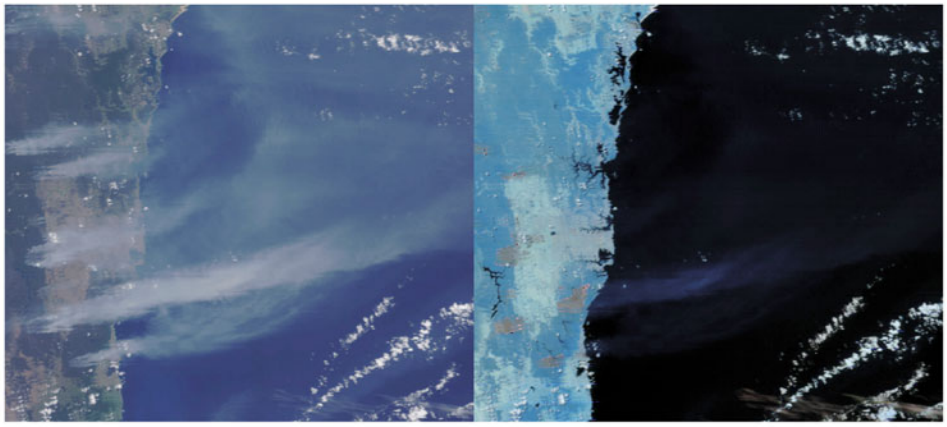

Figure 7.5 MODIS satellite sensor image of Australia, 25 December 2001. Left panel shows smoke from burning wildfires using the wavelength combination of 0.66, 0.55, 0.47 μm to create a true color image. Right panel shows same image but constructed from the wavelength combination of 1.24, 1.63, 2.13 μm. The longer wavelengths are insensitive to the smoke and "see" the surface without interference.

The direct relationship between the adjacency effect blurring the image and the amount of aerosol in that image led to the development of the contrast reduction algorithm. The contrast reduction or the decrease in the difference of apparent reflectance, ρ (as defined in Eq. 7.3) between pixels a certain distance apart (d) is a function of the difference in surface reflectance of the two pixels (ΔR), the total transmission (T_t) and the extinction from the total optical depth of the atmosphere
($\exp(-\tau^*/\mu)$):

$$\Delta\rho_{Ri.j}\ (\mu_0,\mu,\varphi\ ) = \rho_{Ri,j+d} - \rho_{Ri,j} = \Delta R_{i.j} T_t(\mu_0) \exp(-\tau\ ^*/\mu\ ), \tag{7.4}$$

where i and j denote the indices that define the gridded pixel location, μ_o and μ, are cosines of the solar zenith and view zenith angles, and φ is the relative azimuth angle. In Eq. 7.4, we assume that the two pixels are on the same row i and there is a distance d between the two columns j+d and j.

Assuming that the land surface does not vary from day to day, then $\Delta R_{i,j}$ will remain constant and the differences in $\Delta\rho_{i,j}$ from image to image will depend on $T_t(\mu_0)\exp(-\tau^*/\mu)$. The larger the optical depth (τ^*), the smaller the contrast in apparent reflectance ($\Delta\rho_{i,j}$). The procedure requires satellite images from multiple days having the same viewing geometry. The method was applied to deserts using Landsat TM images with identical sun-surface-sensor geometry, with at least one clean image. The hazier images were blurrier. The clean image had more distinct features. These could be compared quantitatively with point-

spread functions and the aerosol retrieved using a LUT and assuming particle properties including size distribution and complex refractive index (Tanré et al., 1988). Besides the ability to retrieve over deserts where the dark target method could not, the contrast reduction method did not require the same level of calibration accuracy because it relied on radiance differences, not the absolute value of the radiance. However, the method requires a fairly fine pixel size. Tanré et al. (1988) demonstrated the technique using 30 m resolution data. AVHRR with its 1 km resolution suffers a 40% reduction in contrast sensitivity, but is still useable according to Holben et al. (1993).

Contrast reduction techniques based on the adjacency effect require multiple images of the same scene and cannot be used in near real time. The scene has to display contrasts at a scale consistent with the sensor resolution and has to be constant during the multiple acquisitions. Perhaps those were the reasons why the algorithm was never applied in any consistent or operational manner. This method was revisited using Landsat and MODIS imagery by Lyapustin et al. (2004).

7.5 Aerosol remote sensing using near UV observations

7.5.1 The UV Aerosol Index

The near-UV capability of aerosol remote sensing using satellite observations is a relatively recent development (Hsu et al., 1996; Herman, J.R. et al., 1997; Torres et al., 1998). As many important scientific discoveries, the UV method was the fortunate unintended result of refinements to the algorithm that since 1978 has been used for the retrieval of atmospheric total column ozone amount using measurements of backscattered ultraviolet (BUV) radiation by the TOMS sensor[1].

The UV Aerosol Index (UVAI) is basically a residual quantity resulting from the comparison between measured and calculated radiances (L^M_λ and L^{cal}_λ respectively) in the range 330–390 nm where gas absorption effects are small. The calculated radiances are obtained using a simple model of the Earth–atmosphere system consisting of a molecular atmosphere bounded at the bottom by a Lambert Equivalent Reflector (LER) (Dave and Mateer, 1967). In this approximation the upwelling UV radiance, L, at the top of the atmosphere is given by the expression

$$L^M(\Omega,\mu,\mu_0,\varphi,p_0) = L_0(\Omega,\mu,\mu_0,\varphi,p_0) + \frac{RF_0T_t(\Omega,\mu,\mu_0,p_0)}{1-RS(\Omega,p_0)}. \tag{7.5}$$

1 The Aerosol Index was the direct result of Dr Pawan K. Bhartia's relentless effort to improve the TOMS total ozone retrieval algorithm. Although Dr Bhartia has never written a first author paper on the subject, he deserves full recognition for the discovery and refinement of this valuable aerosol remote sensing tool.

Equation (7.5) is the same as Eq. (7.1) except for the explicit dependency of the radiative transfer in the UV range on ozone content (Ω) and surface pressure (p_0). A key assumption in this model representation is that the reflectivity R of the column atmosphere's lower boundary is wavelength independent in the near UV. This hypothetical surface approximation is intended to account for the effects of surface, clouds, and aerosols which are not explicitly included in the radiative transfer calculations.

Although the Nimbus 7 TOMS sensor had been in operation since October 1978, the validity of the LER approximation to reproduce the spectral dependence of the measured near-UV radiances was directly tested for the first time in the mid-1990s in the transition from version 6 to version 7 of the TOMS algorithm. The test initially consisted of the calculation of the Lambertian reflectance term by solving for R in Eq. (7.5) at wavelengths in the range 330–380 nm where ozone absorption effects are very small. The Lambertian reflectance of the hypothetical surface accounting for the effects of clouds and aerosol but corrected for Rayleigh scattering is calculated from the expression

$$R_{\lambda_0} = \frac{L^M_{\lambda_0} - L_{o\lambda_0}}{E_{o\_\lambda_0} T_{t\_\lambda_0} + S_{\lambda_0}(L^M_{\lambda_0} - L_{o\lambda_0})}, \tag{7.6}$$

where the dependence variables have been dropped for simplicity. The terms L_o, T_t, E_o and S are obtained from Rayleigh scattering calculations. The term R is calculated at two wavelengths λ_0 and λ, generally 380 and 340 nm, respectively. According to the assumed non-wavelength dependence of the hypothetical Lambertian surface the residual quantity,

$$\Delta R = R_{\lambda_0} - R_{\lambda}, \tag{7.7}$$

should be zero when surface reflection and cloud scattering processes as well as particle scattering and absorption are adequately represented by the simple LER model. On the other hand, non-zero differences are produced when any of the above radiative transfer effects are not adequately represented by the LER approximation as predicted by the early work of Dave et al. (1978).

Examination of global maps of ΔR indicated that UV-absorbing aerosols were by far the most important source of positive differences (Hsu et al., 1996). Hence the term Absorbing Aerosol Index (AAI) or simply, Aerosol Index (AI), was coined to refer to this residual quantity.

The Aerosol Index, initially defined in terms of a reflectivity difference, was later modified to its current form in terms of radiances (Herman, J.R. et al., 1997) to eliminate large angular dependencies at mid-latitudes that made difficult the interpretation of the observed reflectivity differences.

In radiance terms, the AI is calculated as the difference between the measured and the calculated spectral contrast expressed as

$$\mathrm{AI} = -100\left[\log\left(\frac{L^M_{\lambda}}{L^M_{\lambda_0}}\right) - \log\left(\frac{L^{cal}_{\lambda}}{L^{cal}_{\lambda_0}}\right)\right] \tag{7.8}$$

The term $L_{\lambda_0}^{cal}$ is obtained from Eq. (7.5) using R_{λ_0} as calculated from Eq. (7.6) so that

$$L_{\lambda_0}^{cal} = L_{\lambda_0}^{M}.$$

Thus, Eq. (7.8) reduces to

$$\mathrm{AI} = -100 \log\left[\frac{L_{\lambda}^{M}}{L_{\lambda}^{cal}}\right]. \tag{7.9}$$

The log representation is used for historic reasons associated with the ozone retrieval algorithm. A unit AI value represents a 2.3% radiance change. Thus, the AI represents the error in estimating the satellite radiance at λ from radiance measurements at λ_0 assuming a Rayleigh-only atmosphere bounded at the bottom by a spectrally invariant Lambert-Equivalent Reflector.

7.5.2 Aerosol Index properties

The AI is generally positive for absorbing aerosols. The magnitude of the AI associated with absorbing aerosols depends on optical depth, particle size distribution, single scattering albedo, and height of the aerosol layer above surface (Herman, J.R. et al., 1997; Torres et al., 1998). The AI detects absorbing aerosols over water and all terrestrial surfaces including deserts and ice/snow covered surfaces (Hsu et al., 1999). The AI also detects aerosols in cloud–aerosol mixtures, and above cloud decks (Torres et al., 2011).

Non-absorbing aerosols yield negative AI values and their magnitude depends mainly on optical depth and, to a lesser extent, on particle size distribution with small size aerosols (radius less than 0.4 μm) yielding a larger magnitude of AI than do larger particles [Torres et al., 1998].

Since other non-aerosol- related geophysical effects yield a residue (Eq. (7.7)), it is necessary to make use of threshold values to separate the actual aerosol signal from those from other sources. This is particularly true over the oceans where both positive and negative residues of magnitude less than unity are often associated with ocean color effects. For instance, pure water absorption and colored dissolved organic matter in the remote oceans may yield values as high as 0.7, whereas chlorophyll absorption in coastal waters produces negative residues of about the same magnitude. These overlapping effects over the oceans are not a serious limitation for the detection of absorbing aerosols since the magnitude of the AI associated with the long-range transport of smoke and dust is often several times larger than the background ocean signal. However, the use of the negative AI as a proxy of non-absorbing aerosols over the oceans is severely limited as the background oceanic signal is as large (or even larger) than the aerosol related signal, because aerosol optical depths of oceanic non-absorbing aerosols are generally small. The background effect over land areas is not as large as over the oceans although a threshold detection limit must still be used to separate the aerosol signal from that associated with the wavelength dependent

surface albedo in the near-UV region especially over arid and semi-arid regions. The physical meaning of the residue at solar zenith angles larger than about 70° remains uncertain.

The absorbing aerosol index has been used in a variety of applications including the mapping of the global distribution of the frequency of occurrence of carbonaceous and desert aerosols (Herman, J.R. et al., 1997), volcanic ash (Seftor et al., 1997) determination of sources of dust aerosols (Prospero et al., 2002; Yoshioka et al., 2005; Washington et al., 2003), validation of Chemical Transport Models (CTM) (Ginoux et al., 2001; Zender et al., 2003), characterization of biomass burning emissions (Duncan et al., 2003), correction of aerosol effects on total ozone retrieval (Torres and Bhartia, 1999), longterm analysis of global aerosol load (Li et al., 2009), and many more.

7.5.3 Benchmark aerosol events

In addition to the seasonal aerosol activity associated with the annual cycles of agriculture-related biomass burning and desert dust mobilizations across the oceans, the UV Aerosol Index captured synoptic scale episodic aerosol events of natural or anthropogenic origin. A few historic aerosol events that took place prior to the development of the UV remote sensing technique are briefly described here. The satellite depiction of these events in terms of the AI was not observed in real time but the impact on the global environment and the nature of their origin made headlines around the world as major environmental perturbations.

The 1987 Great China Fire

The great China Fire, one of the most destructive fires over the last three decades (Cahoon et al., 1994), was first detected on May 2, 1987 in the Heilongjiang Province of northeastern China. It burned for about three weeks, affecting an area of 1.3 million acres of prime forest and resulting in the loss of over 200 lives and 5000 homes (Cahoon et al., 1994). The Nimbus 7 TOMS Aerosol Index record shows that the synoptic scale smoke plume was transported eastward across the Pacific Ocean, then across Canada and the Atlantic Ocean, reaching as far as central Poland on May 15. Figure 7.6 depicts the spatial extent of the smoke plume on May 10th in terms of the Aerosol Index. The observed discontinuity of the aerosol plume over the Northern Pacific is related to the 24 hr difference between the satellite observations on both sides of the International Date Line.

The 1988 Yellowstone Park Fires

Another historic conflagration of continental proportions was the fires in the United States' Yellowstone National Park located in the states of Wyoming, Montana and Idaho. The Yellowstone Park fires occurred in 1988, the year when the driest summer in the park's recorded history took place. About 793,000 acres or 36% of the park's area burned over a two month period from July to September (Romme and Despain, 1989). In spite of the huge efforts in containing the fires, it was only the first snowfall of early September that began dampening the fires although the last of the smoldering flames were not extinguished until November. Over much of this period, a dense smoke layer covered a large fraction of the Continental US, Canada and Northern Mexico. The Nimbus 7 TOMS Aerosol Index image in Figure 7.7 depicts the re-circulated carbonaceous aerosol layer on September 9th. Nim-

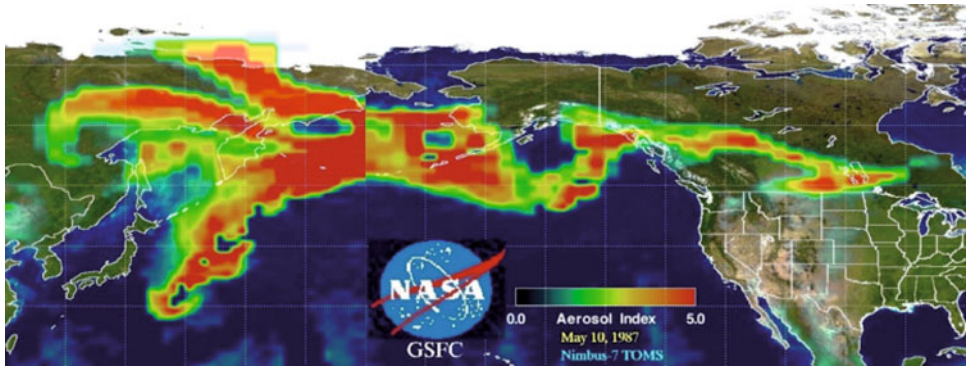

Figure 7.6 May 10, 1987 snapshot of the aerosol layer generated by the Great China Fire in terms of the TOMS Aerosol Index.

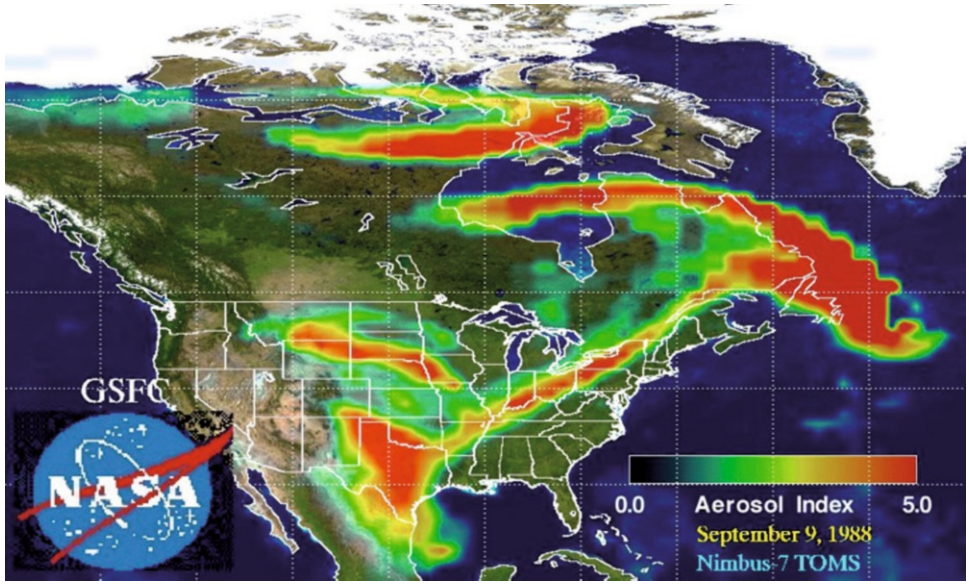

Figure 7.7 Geographical extent of the Yellowstone Park fires plume registered by the Nimbus7 TOMS aerosol Index on September 9, 1988.

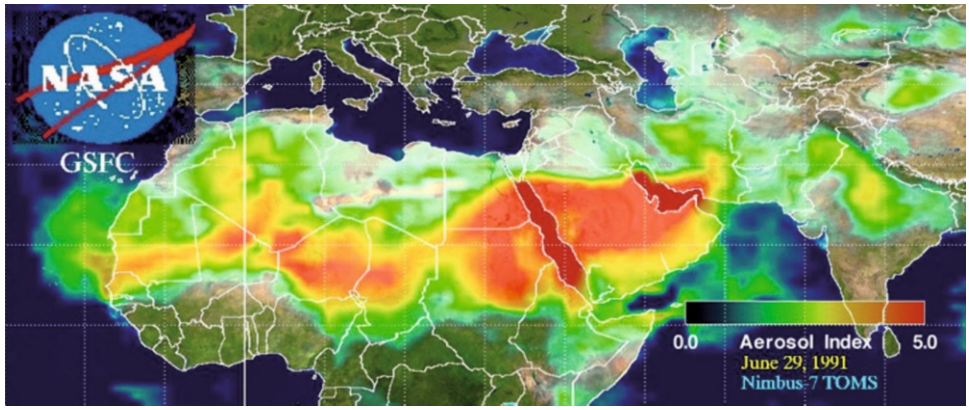

Figure 7.8 The east-to-west extent across Northern Africa of the Kuwaiti Oil fires on June 29, 1991 as seen by TOMS.

bus 7 TOMS data shows that smoke from the Yellowstone Park fires was also transported across the Atlantic Ocean, reaching Western Europe.

The 1991 Gulf War oil fields fires

In the aftermath of the January 1991 armed conflict in Kuwait, over 700 oil wells were set ablaze. The resulting environmental catastrophe produced hundreds of oil spills across the Kuwaiti desert. The oil fires burned for over a 10-month period. The last fire was reportedly extinguished in November 1991. Although it was initially believed that most of the smoke was confined to the Persian Gulf region (Cahalan, 1992), Aerosol Index observations by the Nimbus-7 TOMS sensor would show that the massive smoke plume was actually transported thousands of kilometers away from the source region across Northern Africa following the same path in which Saharan dust is annually mobilized out of the Saharan desert and across the North Atlantic Ocean to the Americas. The plume from the Kuwaiti oil fires may have possibly reached the Pacific Ocean as suggested by Lowenthal et al. (1992) based on observations in Hawaii. The long-range westward transport of aerosol material generated in Kuwait is clearly shown in Figure 7.8 on June 29, 1991.

7.5.4 Application to other sensors

Since its inception, the UV Aerosol Index has been implemented as either an operational or research product in inversion algorithms applied to instruments with UV observing capability such as GOME, GOME-2, SCIAMACHY, and OMI. Some of these products and the applications stemming from their use are described for GOME (Gleason et al., 1998; de Graaf et al., 2005), SCIAMACHY (de Graaf et al., 2007; Penning de Vries et al., 2009), OMI (Torres et al., 2007; Ahn et al., 2008; Dirksen et al., 2009). The near-UV advantages

for aerosol detection, i.e. sensitivity to aerosol absorption and low surface albedo, are used in a retrieval algorithm as described in the following section.

7.5.5 Quantitative use of near-UV observations

The information content of the Aerosol Index is turned into quantitative estimates of aerosol extinction optical depth (τ) and single scattering albedo(ϖ) at 380 nm by application of an inversion algorithm to TOMS near-UV observations (Torres et al., 1998). The τ and ϖ quantities are derived using a standard inversion algorithm that uses pre-computed reflectances for a set of assumed aerosol models. Three major aerosol types are considered: desert dust, carbonaceous aerosols associated with biomass burning, and weakly absorbing sulfate-based aerosols. Each aerosol type is represented by seven aerosol models of varying single scattering albedo, for a total of 21 microphysical models. For a chosen aerosol type, represented by a sub-set of seven aerosol models, the extinction optical depth and single scattering albedo are retrieved by examining the variability of the relationship between the 340–380 nm spectral contrast and the 380 nm reflectance. Since the retrieval procedure is sensitive to aerosol vertical distribution, the aerosol layer height must be assumed. The choice of vertical distribution varies with aerosol type and location (Torres et al., 2002). Surface reflectance is prescribed using an existing climatological database derived from the long-term TOMS reflectivity record (Herman and Celarier, 1997). The near-UV retrieval algorithm was applied to the Nimbus 7 (1979–1992) and Earth Probe (1996–2001) TOMS records (Torres et al., 2002) as part of the Global Aerosol Climatology Project. The TOMS aerosol climatology was the first global record of atmospheric aerosol load that provided data over both the oceans and the continents. Figure 7.9 shows the combined Nimbus 7-Earth Probe TOMS aerosol optical depth record from 1979 to 2001. No TOMS measurements were available during the 1993–1996 three-year gap.

The Deep Blue algorithm (Hsu et al., 2006) was inspired by the proven retrieval capability in the UV over arid and semi-arid areas. Although strictly not in the UV, at the MODIS 412 nm channel deserts appear sufficiently darker than at the other available MODIS wavelengths allowing the retrieval of aerosol properties. The Deep Blue application, currently used in the operational MODIS algorithm for the retrieval of aerosol optical depth over deserts, is discussed in detail in Chapter 8.

7.6 Multiangle, polarization and geosynchronous capabilities

7.6.1 Multiangle

The above discussion of the evolution of the occultation, dark target and UV methods outlines the historical progression of the three main methods of satellite aerosol remote sensing that resulted in operational or semi-operational products, producing a long time series. In addition to these three historical lines were other methods making use of additional capabilities inherent in other satellite sensors. Primarily, these include multiangle observations of the same pixel, polarization and multiple observations within the same day. These

additional capabilities were explored during the same time period when data from AVHRR and TOMS were being used to derive aerosol information. Here, we give a brief overview of these early explorations that in some cases became predecessors to the EOS era satellite sensors that were designed specifically with aerosol in mind.

Although the concept was proposed earlier (Martonchik and Diner, 1992), multiangle aerosol retrievals began with the Along-Track Scanning Radiometer-2 (ATSR-2) (Stricker et al., 1995). This instrument, launched in 1995 on the European Remote Sensing Satellite (ERS) provided the first opportunity to view each Earth scene from multiple angles. ATSR-2 used a conical scanning mechanism that views a particular scene first at approximately 56° in the forward direction and then 2 minutes later from nadir. The instrument measured in seven wavelengths, three in the infrared and not used for aerosol retrievals, and four at 0.555, 0.659, 0.865, and 1.6 μm that were used for aerosol retrieval. Algorithms to derive aerosol from these multiwavelength multiangle views were developed by J.P. Veefkind and his co-authors (Veefkind et al.,1998, 1999). In part based on work by Flowerdew and Haigh (1996), the method relies on the ATSR-2 natural viewing geometry to avoid the surface hotspot from vegetation and assumes a Lambertian surface. The retrieval is based on the radiance measurement at the top of the atmosphere given by Eq. (7.1). Because there are only two geometries, forward and nadir, the geometrical dependency can be denoted by 'f' and 'n' superscripts. Furthermore, the method assumes that the surface reflectance

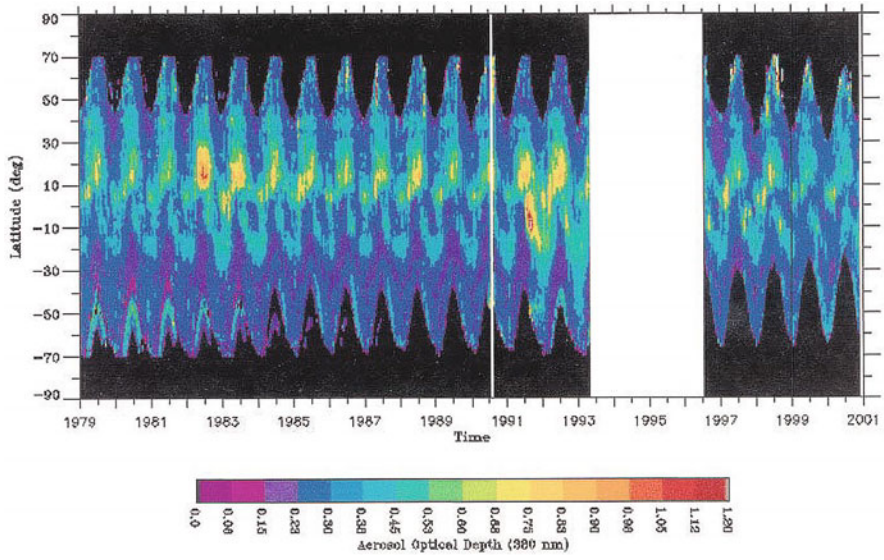

Figure 7.9 TOMS 380 nm AOD 1979–2001 global record from Torres et al. (2002). Reproduced with permission from the American Meteorological Society.

viewed at the forward angle is directly proportional to the reflectance viewed at nadir, such that

$$R^{f}(\lambda) = k \bullet R^{n}(\lambda), \tag{7.10}$$

where R is the Lambertian surface reflectivity of Eq. (7.1), but designated either for the forward view R^{f} or the nadir view R^{n}, and k is the ratio between forward and nadir surface reflectivity, which is assumed to be invariant with wavelength. The method assumes that the atmosphere dominated by fine mode aerosol is effectively invisible to radiation in the short wave infrared (Figure 7.4 and Kaufman et al., 1997a), and uses the measured top-of-atmosphere radiances in the 1.6 μm channel to calculate k. The k parameter is then applied to the visible wavelengths. Thus, the surface reflectance model is known even if the surface reflectance is not, and the difference in measured radiance of the two geometries is dependent only on parameters that are a function of the aerosol optical depth, τ. The method requires an assumed aerosol model that provides the intrinsic aerosol optical properties, and a Look-Up Table to match with the measured radiance differences.

The ATSR-2 method was applied and validated on the east coast of the United States (Veefkind et al., 1998). Subsequent applications of the dual-view method included aerosols over Europe, India and Africa (Gonzales et al., 2000; Robles-Gonzales and Leeuw, 2006, 2008). A similar method was adapted to the Advanced Along Track Scanning Radiometer AATSR (Grey et al., 2006). While the ATSR-2 retrievals never created a long time series of global aerosol measurements, as did AVHRR and TOMS, the ATSR-2 retrievals did pioneer the path towards multiangle measurements in general. Later, the Multiangle Imaging Spectro Radiometer (MISR) would continue the tradition of using multiple angles to derive aerosol information and create a long-term operational data base of aerosol products.

7.6.2 Polarization

Polarization adds significant capability to aerosol retrieval, especially when combined with multiangle and multiwavelength measurements. Early studies based on ground-based measurements and planetary observations suggested polarization could play an important role in aerosol remote sensing (Deuzé et al., 1988; Hansen and Hovenier, 1974). Aerosol retrievals using polarization were explored theoretically and were found to provide significant advantage in terms of information content (Mishchenko and Travis, 1997) and in being much less sensitive to surface properties (Leroy et al. 1997) than intensity measurements alone.

The first Earth-viewing space instrument employing polarization was the Polarization and Directionality of the Earth Reflectance (POLDER) that was launched in 1996. POLDER is a wide field-of-view instrument that images ±43° and ±51° along-track and cross-track, respectively, and produces a pixilated 242×274 pixel image using a CCD detector array (Deschamps et al., 1994). The result is a series of images as the instrument moves along its orbit, with several images partially overlapping, creating multiple views of the same pixel. A filter wheel provides measurements at 9 channels from 443 nm to 910 nm, with three of those channels each measured at three polarization states (Deschamps et al., 1994). The aerosol retrieval algorithm makes use of this information to derive aerosol

optical depth and Ångström exponent over ocean (Deuzé et al., 1999) and the fine mode aerosol optical depth over land (Herman et al., 1997; Deuzé et al., 2001). There have been three POLDER instruments in space. The first two were of relatively short duration, August 1996 to June 1997 and December 2002 to September 2003, respectively, due to malfunctions on the ADEOS satellites that provided the platform for these instruments. The third POLDER was launched on the PARASOL satellite in December 2004. PARASOL joined the international afternoon constellation of satellites in polar orbit and remained in this constellation until December 2009. As of this writing, PARASOL continues collecting and transmitting data. Because POLDER/PARASOL is a contemporary of the other Terra and A-Train sensors, a more detailed description of the retrieval algorithm is left for Chapter 8.

7.6.3 Retrievals from geosynchronous satellites

Geosynchronous satellites offer fine temporal resolution observations of aerosols on a regional basis so that particle plumes can be monitored over the course of the day. The historical difficulty with using these sensors for aerosol retrievals has been the uncertain calibration. Fraser et al. (1984) used a vicarious calibration method to calibrate the visible channel on GOES-1, and Knapp and Vonder Haar (2000) did the same to calibrate GOES-8. Fraser et al. (1984) and Knapp et al. (2002) describe a technique that uses a composite method to fix the surface reflectance for every time of day of observation. The minimum reflectance for each pixel for each time of day of a two-month period was corrected for gaseous absorption and a minimum background aerosol optical depth. The result was an estimate of the surface reflectance that was assumed invariant over the entire period of interest. Measured reflectance that exceeded this minimum reflectance was assumed to be due to aerosol loading. A Look Up Table with an assumed aerosol model provided the means to retrieve the aerosol optical depth, using a basic dark target approach, but with a known surface reflectance. Other similar attempts include Wang et al. (2003) for GOES and Popp et al. (2007) for the Spinning Enhanced Visible and Infrared Imager (SEVIRI) on the geosynchronous Meteosat Second Generation (MSG) satellite. The procedure was made operational at NOAA under the name GOES Aerosol/Smoke Product (GASP) (Prados et al., 2007).

7.7 Summary

The primary space-based passive methods to derive aerosol are:

(1) Occultation methods that measure the extinction of solar radiation and provide vertical profiles of aerosol extinction through the stratosphere. These methods have a long history and make possible a multi-decadal time series that has illustrated the effect of explosive volcanic eruptions on stratospheric aerosol.

(2) Dark target methods that retrieve the aerosol optical depth through the total column of the atmosphere. These methods have to overcome issues with calibration of the sensor, and they require *a priori* assumptions of aerosol optical properties and surface reflect-

ance. At best, the dark target retrieval can retrieve aerosol optical depth and some information of spectral dependence or particle size. Applied to AVHRR, dark target methods have provided a long time series over the oceans that suggest trends in global aerosol loading, but questions concerning sampling, drift and merging of records from different satellites prevent the long-term AVHRR trend from being universally accepted.

(3) UV methods also retrieve through the total column of the atmosphere, although their standard product is a robust Aerosol Index (AI) that provides a useful qualitative measure of aerosol loading and aerosol light absorption. Retrievals of quantitative aerosol optical depth can also be derived, but with *a priori* assumptions of aerosol optical properties, surface reflectance and aerosol layer height. However, the UV method is less sensitive to surface reflectance than the dark target methods. The UV method applied to the TOMS data record provides our longest existing record of aerosol optical depth information.

Besides these three main methods applied to the SAM/SAGE, AVHRR and TOMS measurements, respectively, to produce long aerosol time series, other methods have been developed to make use of multiangle, polarization and geosynchronous capabilities. These satellite aerosol products applied to data collected in the 1980s and 1990s made way for the era of the modern sensors that began with the launch of Terra in late 1999. Occultation, dark target and UV methods, embellished with better calibration, polarization, more wavelengths and more angles provide the basis of EOS-era satellites of the 2000s.